Interface Excess and Polymorphic Stability of Nanosized Zirconia-Magnesia

Ricardo H. R. Castro,*,† Paulo J. B. Marcos,‡ Annick Lorriaux,§ Marlu C. Steil,|| Léon Gengembre,§ Pascal Roussel,§ and Douglas Gouvêa⊥

Department of Materials Engineering, FEI University Center, São Bernardo do Campo, SP 09850-901, Brazil, Faculdade de Tecnologia de São Paulo, Praça Coronel Fernando Prestes 30, São Paulo, SP 01124-060, Brazil, Unité de Catalyse et Chimie du Solide−UMR CNRS 8181, Ecole Nationale Superieure de Chimie de Lille Bat C7a, BP 90108 F-59652, Villeneuve d'Ascq, France, Laboratoire d'Electrochimie et de Physico-chimie des Matériaux et des Interfaces (LEPMI), CNRS, Universite Joseph Fourier, INPG, 1130 Rue de la Piscine, BP 75, 38402 Saint Martin d'Hères Cedex, France, and Department of Metallurgical and Materials Engineering, University of São Paulo, Avenida Prof. Mello Moraes, 2463, São Paulo, SP 05508-900, Brazil

Received December 17, 2007. Revised Manuscript Received February 21, 2008

Controlling the phase stability of ZrO_2 nanoparticles is of major importance in the development of new ZrO_2-based nanotechnologies. Because of the fact that in nanoparticles the surface accounts for a larger fraction of the total atoms, the relative phase stability can be controlled throughout the surface composition, which can be tuned by surface excess of one of the components of the system. The objective of this work is to delineate a relationship between surface excess (or solid solution) of MgO relative to ZrO_2 and the polymorphic stability of $(ZrO_2)_{1-x}-(MgO)_x$ nanopowders, where $0.0 \leq x \leq 0.6$. The nanopowders were prepared by a liquid precursor method at 500 °C and characterized by N_2 adsorption (BET), X-ray diffraction (XRD), X-Ray photoelectron spectroscopy (XPS), and Raman spectroscopy. For pure ZrO_2 samples, both tetragonal and monoclinic polymorphs were detected, as expected considering the literature. For MgO molar fractions varying from 0.05 to 0.10, extensive solid solution could not be detected, and a ZrO_2 surface energy reduction, caused by Mg surface excess detected by XPS, promoted tetragonal polymorph thermodynamic stabilization with relation to monoclinic. For MgO molar fractions higher than 0.10 and up to 0.40, Mg solid solution could be detected and induced cubic phase stabilization. MgO periclase was observed only at $x = 0.6$. A discussion based on the relationship between the surface excess, surface energy, and polymorph stability is presented.

Introduction

The phase stability in nanosized materials is strongly dependent on a surface term due to the relatively large fraction of surface atoms.[1] Therefore, in addition to the bulk free energy, surface energy has been included as a relevant component in phase stability diagrams to predict stable polymorphs in nanopowders with phase transformations such as ZrO_2, Al_2O_3, and TiO_2.[2–4]

However, more than understanding the stability reasons, it is technologically important to find efficient tools to control these phase transformations in the desired level. A common tool is the usage of ionic additives during the synthesis of the nanoparticles.[5–7] This method is efficient at controlling transformation temperatures and nanostructures of many systems; nevertheless, the mechanisms behind this efficiency are not always clear, and phenomenological explanations are usually given exclusively on the basis of kinetics grounds.

A recent work reported that, at least for Al_2O_3 nanoparticles, ionic additives used as transformation controllers can act in both kinetic and thermodynamics basis.[8] Hence, because we are dealing with a nanosized material, both surface and bulk energies have importance in the polymorphic stability, and the effect of the additives must be considered in both energies. This was demonstrated discussing the effect of Zr in raising γ to α-alumina transformation temperature.[8] Using drop-solution calorimetry, it was reported that 2 mol % Zr decreases the surface energy of γ-alumina from 2.04 to 1.04 J m^{-2}. This causes a drastic stabilization of gamma with relation to alpha, increasing the transformation temperature, regardless of the kinetics effects. The main reason for this remarkable surface energy decrease

* Corresponding author. E-mail: rhrcastro@fei.edu.br. Phone: 55 11 43532900. Fax: 55 11 41095994.
† FEI University Center.
‡ Faculdade de Tecnologia de São Paulo.
§ Ecole Nationale Superieure de Chimie de Lille Bat C7a.
|| Universite Joseph Fourier.
⊥ University of São Paulo.

(1) Gleiter, S. H. *Acta Mater.* **2000**, *48*, 1.
(2) Navrotsky, A. *Abstr. Am. Chem. Soc.* **2003**, *225*, U939.
(3) McHale, J. M.; Auroux, A.; Perrotta, A. J.; Navrotsky, A. *Science* **1997**, *277*, 788.
(4) Pitcher, M. W.; Ushakov, S. V.; Navrotsky, A.; Woodfield, B. F.; Li, G. S.; Boerio-Goates, J.; Tissue, B. M. *J. Am. Ceram. Soc.* **2005**, *88*, 160.
(5) Okada, K.; Hattori, A.; Kameshima, Y.; Yasumori, A.; Das, R. N. *J. Am. Ceram. Soc.* **2000**, *83*, 1233.
(6) Pijolat, M.; Dauzat, M.; Soustelle, M. *Thermochim. Acta* **1987**, *122*, 71.
(7) Rong, T. J.; Huang, X. M.; Wang, S. W.; Zhao, S. K.; Guo, J. K. *J. Am. Ceram. Soc.* **2002**, *85*, 1324.
(8) Castro, R. H. R.; Ushakov, S. V.; Gengembre, L.; Gouvea, D.; Navrotsky, A. *Chem. Mater.* **2006**, *18*, 1867.

10.1021/cm703599r CCC: $40.75
Published on Web 04/24/2008

is the spontaneous formation of a surface excess of Zr in the alumina matrix. In fact, there is no reason to believe this behavior is restricted to alumina powders, and similar effects may occur for $BaTiO_3$, ZrO_2, and other systems with solid phase transformations. Hence, if an additive is prone to segregate on the surface of another, one may expect that it can be used as an instrument to control its surface energy, and therefore, the polymorphic stability of nanosystems that are highly dependent on it.

ZrO_2 is typical system where this hypothesis could be tested observing the presence of surface excesses and relating to the polymorphic stabilities. Recent calorimetric measurements have directly shown the role of surface energies in the relative thermodynamic stability of ZrO_2 polymorphs (monoclinic, m; tetragonal, t; and cubic, c),[4] as predicted earlier by Garvie et al.[9] The relatively high surface energy of m-ZrO_2 ($\sim$6.4 J m^{-2}) restricts its stability to surface areas lower than $\sim$20 m^2 g^{-1}, also known as critical surface area. On the other hand, because t-ZrO_2 has a relatively low surface energy ($\sim$2.1 J m^{-2}), despite the high transformation enthalpy from m- to t-ZrO_2 ($\Delta H_{m-t} \approx 10$ kJ mol^{-1}), the surface term decreases the system total energy and enable its stability at surface areas higher than $\sim$20 m^2 g^{-1}. The surface energy for pure c-ZrO_2 polymorph has also been computed as $\sim$3.2 J m^{-2}.[10] The well-known instability of this polymorph thus appears from the fact that ΔH_{m-c} is $\sim$13.5 kJ mol^{-1};[11] thereafter, both m- and t-ZrO_2 will be more stable at room temperature.

Dopants (Mg, Y, and Ca) are commonly used to stabilize the cubic polymorph with relation to t- and m-ZrO_2 at room temperature.[11–13] The explanation for this stabilization is usually discussed based on the effect of the cations in both atomic and electronic structures of the ZrO_2 crystals.[12] This can be thermodynamically associated with bulk enthalpy modifications, changing the relative critical surface area, but without properly addressing a surface term.

When dopants tend to segregate to the surface of nanoparticles, the consequent surface energy lowering predicted by Gibbs eq 1[14] will also affect the relative stability of the polymorphs.[8]

$$\Gamma_2 = -\frac{d\gamma}{RTd\ln c_2} \quad (1)$$

where Γ_2 is the surface excess in a two component system, γ is the surface energy, R is the gas universal constant, T is the temperature, and c_2 is the solubility of the component.

Despite the simplified assumptions of Gibbs approach, that does not allow a quantitative analysis in a crystalline system; a qualitative analysis is still reasonable using this equation. For example, the average surface energy of c-ZrO_2 containing 14 mol % Y has been computed to be almost half the value for pure c-ZrO_2 due to yttrium surface excess.[10] To the best of or knowledge, surface energy measurements or simulations in ZrO_2−MgO systems have not been carried out; however, surface segregation of Mg in ZrO_2 powder has been detected in ZrO_2−10.4 mol % MgO powders,[7] suggesting that only a fraction of MgO is in extensive solid solution and that the surface energy may also be reduced because of surface excess, as reported in some other oxide systems.[1,8,15]

Even though ZrO_2−MgO system has been the object of many works in the past decades,[12,16–19] some contradictory results about the relative polymorphic stability have been published. This can be associated with sample heterogeneities or the absence of a surface excess term discussion. The aim of this work is to delineate the relationship between MgO surface excess (and consequent surface energy reduction) and the stability of ZrO_2 polymorphs at 500 °C. $(ZrO_2)_{1-x}$ − $(MgO)_x$ nanopowders with $0.0 \leq x \leq 0.6$ were synthesized by a liquid precursor method to ensure high homogeneity, and the stable polymorphs were identified by XRD and Raman spectroscopy. The distribution of the components (Mg and Zr) was studied by XPS to identify surface excess and/or solid solutions and the powder nanostructure were analyzed by XRD size-strain line-broadening analysis, He picnometry, SEM-FEG, and specific surface area (S_{BET}) analysis. The greater objective is therefore to prove that, indeed, the surface excess determines the polymorphic stability throughout the modifications of the surface energies, in addition to kinetic effects.

Experimental Section

Synthesis. $(ZrO_2)_{1-x}$ − $(MgO)_x$ nanopowders, where $x = 0.000$, 0.010, 0.050, 0.086, 0.100, 0.200, 0.300, 0.400, 0.500, and 0.600, were synthesized by a liquid precursor method derived from the Pechini's patent.[20] The liquid precursor guarantees high homogeneity of dopants distribution, and with appropriate heat treatment, an equilibrium state for the composition is obtained.[21] The process can be briefly described as follows: (a) the cationic precursors were introduced into an ethylene glycol (60 wt %) and citric acid (40 wt %) solution. $Zr(CO_3)_2 \cdot xH_2O$ (Alfa Aesar, P.A.) and MgO (Synth, P.A.) were used as the cationic precursors. The amounts of precursors were calculated to achieve the desired molar concentrations. (b) The prepared solution was heated up to 120 °C to promote polyesterification, i.e., polymerization between citric acid and ethylene glycol giving rise to a polymer chain with sites available to form chelates with the present ions. These sites randomically react with Zr or Mg ions forming the complexes. (c) The obtained liquid precursor was thermally treated at 450 °C for 4 h under air atmosphere and a dry carbon rich powder was obtained. After grinding, the powder was treated for 15 h at 500 °C to guarantee

(9) Garvie, R. C.; Goss, M. F. *J. Mater. Sci.* **1986**, *21*, 1253.
(10) Ballabio, G.; Bernasconi, M.; Pietrucci, F.; Serra, S. *Phys. Rev. B* **2004**, *n/a*, 70.
(11) Molodetsky, I.; Navrotsky, A. *Z. Phys. Chem.* **1998**, *207*, 59.
(12) Stefanovich, E. V.; Shluger, A. L.; Catlow, C. R. A. *Phys. Rev. B* **1994**, *49*, 11560.
(13) Ushakov, S. V.; Brown, C. E.; Navrotsky, A. *J. Mater. Res.* **2004**, *19*, 693.
(14) Chiang, Y.-M.; Birnie, D.; Kingery, W. D., *Physical Ceramics−Principles for Ceramic Science and Engineering*; John Wiley & Sons Inc.: New York, 1997.
(15) Castro, R. H. R.; Hidalgo, P.; Coaquira, J. A. H.; Bettini, J.; Zanchet, D.; Gouvea, D. *Eur. J. Inorg. Chem.* **2005**, *11*, 2134.
(16) Rong, T. J.; Hunag, X. X.; Guo, J. K.; Wang, S. W. *J. Inorg. Mater.* **2003**, *18*, 238.
(17) Muccillo, R.; Saito, N. H.; Muccillo, E. N. S. *Mater. Lett.* **1995**, *25*, 165.
(18) Muccillo, R.; Muccillo, E. N. S.; Saito, N. H. *Mater. Lett.* **1998**, *34*, 128.
(19) Zavodinsky, V. G. *Phys. Solid State* **2004**, *46*, 453.
(20) Pechini, M.; U.S. Patent 3 330 697, July11, 1967.
(21) Gouvea, D.; Varela, J. A.; Longo, E.; Smith, A.; Bonnet, J. P. *Eur. J. Solid State Inorg. Chem.* **1993**, *30*, 915.

total carbon elimination and an energetically stable particle size and distribution of the dopants.

Characterization Techniques. X-ray diffraction patterns (XRD) were collected using a Bruker AXS instrument (model D8 Advance, Cu Kα radiation, $\lambda = 1.5406$) to determine the crystallographic phases and to measure the microstructural effects (size and/or strain) of the particles. It is known that broadening of diffraction lines occurs for two main reasons: instrumental effects and physical origins. The latter can be roughly divided into diffraction-order-independent (size) and diffraction-order-dependent (strain) broadening in reciprocal space. In this paper, we used a simplified integral-breadth method that assumes either a Gaussian or Lorentzian function for a size- and/or strain-broadened profile. Thus, the construction of Halder−Wagnet plots[22] was undertaken using a standard software, taking care of the instrumental broadening effects (the Standard Reference Material SRM660a LaB_6 from the National Institute of Standards, NIST, was used to account for the diffractometer broadening). As reviewed by Langford,[23] considering a Voigtian[24] profile, the integral breadth β is related to the size D and/or strain ε through the relation

$$(\beta*/d*)^2 = D^{-1}\beta*/(d*)^2 + (\varepsilon/2)^2 \qquad (2)$$

Therefore, the intercept of the plot $(\beta*/d*)^2$ versus $\beta*/(d*)^2$ gives the mean value of the lattice strain ε, and the slope gives the mean apparent size D.

Since XRD technique was not able to precisely differ tetragonal from cubic polymorphs, Raman spectroscopy was also carried out to determine the stable phases after synthesis. The Raman spectra were obtained at room temperature using 647.1 nm exciting wavelength from a Spectra Physics Kr^+ ion laser. The scattered light was analyzed with an XY Raman Dilor spectrometer equipped with an optical multichannel charge coupled device liquid nitrogen-cooled detector. The spectral resolution was ~0.5 cm^{-1} in the 125−1300 cm^{-1} required range.

Surface analyzes were performed using the VG ESCALAB 220XL spectrometer. Al kα nonmonochromatized line (1486.6 eV) was used for excitation with a 300W-applied power. The analyzer was operated in a constant pass energy mode (40 eV). Binding energies were referenced to the Zr_{3d}[5] core level (182.1 eV) of ZrO_2 and to the Mg_{1s} core level (1304 eV) of MgO. These references were consistent over the whole MgO-ZrO_2 range within 0.2 eV. The vacuum level during the experiment was $<1 \times 10^{-7}$ Pa. The powdered catalysts were pressed as thin pellet onto indium foil. Experimental quantification was obtained using the Eclipse software provided by ThermoVG Scientific

The specific surface area (S_{BET}) measurements were performed with a Gemini III 2375 surface area analyzer (Micromeritics, Norfolk, MA). The powders were treated at 200 °C for 4 h under a vacuum ($>1 \times 10^{-5}$ mmHg) before each analysis to decrease the effect of physisorbed water that could decrease the measured area. The measurements were carried out using N_2 as absorbent and using 5 points to use the BET (Brunauer−Emmett−Teller) approach. The samples mass was always higher than 0.1 g to ensure low uncertainties associated with the samples mass. This is a standard procedure considered efficient to measure the specific surface area of oxides such as ZrO_2,[4] Al_2O_3,[8] SnO_2,[25] and others.

The density of the compounds was performed on the specimens heated at 110 °C for 1 h with a helium pycnometer (Micrometrics-AccuPyc 1305). These data were used to estimate the surface energies using Ostwald ripening approach.[14] The morphology of the powders particles was examined using a scattering electron microscope Hitachi S4700 (SEM-FEG) using high resolution mode with 5.0 or 7.0 kV. TEM image was acquired in a JEM 3010 URP microscope using 300 keV (0.17 nm resolution).

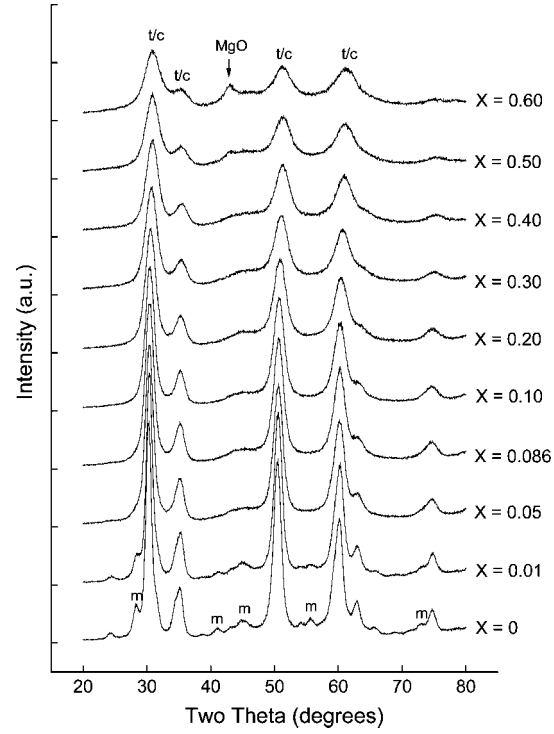

Figure 1. XRD diffraction patterns for ZrO_2 nanopowders containing different amounts of MgO. X is the MgO molar fraction; (t/c) indicates the peaks that cannot be clearly distinguished between tetragonal and cubic phase by XRD, and (m) indicates the monoclinic phase.

Results and Discussion

Figure 1 shows XRD patterns for $(ZrO_2)_{1-x} - (MgO)_x$ nanopowders, with x varying from 0.00 to 0.60, prepared by the liquid precursor method. For both pure ZrO_2 and ZrO_2 containing 1 mol % MgO ($x = 0.01$), one observes traces of monoclinic polymorph in addition to diffraction peaks that cannot be clearly distinguished between t- or c-ZrO_2. For x varying from 0.05 to 0.30, the peaks attributed to t- or c-ZrO_2 decrease in intensity, possibly because of the particle size decreasing. MgO periclase traces are observed only for MgO fractions higher than 0.50.

Figure 2 shows Raman spectra recorded under microscope for pure and doped ZrO_2 samples. Confirming the XRD data, both monoclinic and tetragonal polymorphs were detected in the spectra for ZrO_2 without MgO. m-ZrO_2 is characterized by the doublet at 179 and 191 cm^{-1}, whereas the two distinct bands at 147 and 269 cm^{-1} are assigned to the tetragonal phase.[26–29] For 0.05 MgO sample, the intensities of char-

(22) Halder, N. C.; Wagner, C. N. J. *Acta Crystallogr., Sect. A* **1966**, *20*, 312.
(23) Langford, J. I. In *Proceedings of the International Conference on Accuracy in Powder Diffraction II*, May 26−29, 1992, Gaithersburg, MD; Prince, E., Stalick, J. K., Eds.; National Institute of Standards and Technology: Washington, D.C., 1992; p 26.
(24) Daly, R.; Khotouni, M.; Kolsi, W.; Njah, N. *Phys. Status Solidi A* **2006**, *9*, 3325.
(25) Hidalgo, P.; Castro, R. H. R.; Coelho, A. C. V.; Gouvea, D. *Chem. Mater.* **2005**, *17*, 4149.
(26) Sobol, A. A.; Voronko, Y. K. *J. Phys. Chem. Solids* **2004**, *65*, 1103.

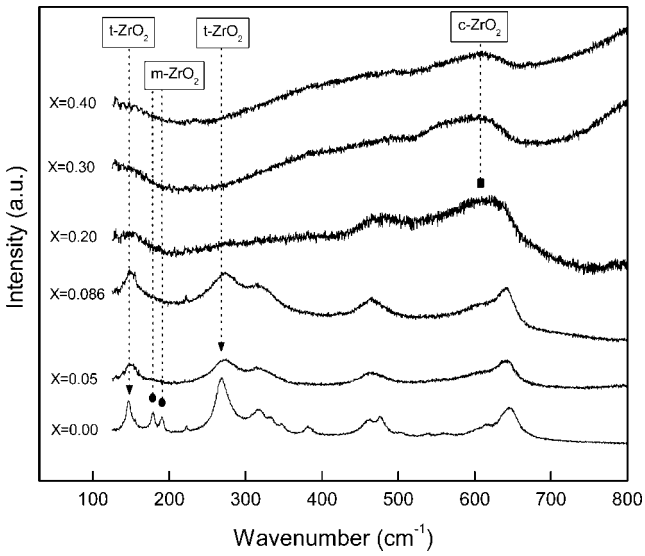

Figure 2. Raman Spectroscopy data for ZrO_2 based samples, X indicates the MgO molar fractions. t-ZrO_2, m-ZrO_2, and c-ZrO_2 indicate the characteristic bands for tetragonal, monoclinic, and cubic zirconia, respectively.

acteristic peaks attributed to monoclinic cell are weaker, but still observed. For MgO content 0.086, t-ZrO_2 polymorph is stable and m-ZrO_2 is no longer detected, which is consistent with data reported for 10.4 mol %-doped zirconia powder prepared from coprecipitation.[7] The spectral features can also contribute to the understanding of the distribution of the phases. Since the spectrum is close to the solid solution of ZrO_2 tetragonal type, one may suggest that the monoclinic polymorph surrounds t-ZrO_2 particles as suggested previously.[30–32] For $x = 0.20$ and 0.30, one observes only traces of distorted t-ZrO_2 structure and mainly c-ZrO_2 (Figure 2). The weak broadband around 150 cm^{-1} identifies the distorted t-ZrO_2, together with the band at 273 cm^{-1} and low intensity bands at 467 and 486 cm^{-1}. c-ZrO_2 is identified by the characteristic broadband at 610 cm^{-1}.[26,27] For $x = 0.40$, bands attributed to t-ZrO_2 are no longer observed and the MgO characteristic one (at 1150 cm^{-1}) is still not detected. Only the characteristic band assigned to c-ZrO_2 is observed with a maximum observed at 600−610 cm^{-1} frequency values. Figure 3 compiles the relative stability of the $(ZrO_2)_{1-x} - (MgO)_x$ polymorphs as a function of the composition considering both XRD and Raman scattering measurements.

Because the polymorphic stability depends on the relationship between the surface and the bulk enthalpies and their relative amounts,[9] Mg location will drive the stable polymorph if surface excess is observed, as previously shown for Al_2O_3 nanopowders doped with Zr or Mg.[8] Table 1 shows XPS quantification carried out in $(ZrO_2)_{1-x} - (MgO)_x$ nanopowders. The atomic Mg_{1s}/nZr_{3d} ratio is particularly representative of Mg ions dispersion in the uppermost surface layers, whereas nMg_{2s}/nZr_{3d} can be attributed to inner dispersion (bulk solid solution). The main information from the presented data is the higher values for nMg_{1s}/nZr_{3d} when compared to the bulk ones, suggesting surface excess of Mg that persists throughout the studied concentration range. Moreover the nMg_{1s}/nMg_{2s} ratio also shows that the surface Mg enrichment is more pronounced for the lower values of x than for the higher ones ($x = 0.5$ and 0.6) which are not so different from the MgO value ($x = 1$). Combining the XPS data with the polymorphic relative stability from schematically shown in Figure 3, the surface excess is thus observed when t-ZrO_2 with traces of monoclinic polymorph is stable ($x = 0.05$); when only t-ZrO_2 is detected ($x = 0.086$); when both t- and c-ZrO_2 are stable ($x = 0.20$ and 0.30); and when only c-ZrO_2 is observed ($x = 0.40$).

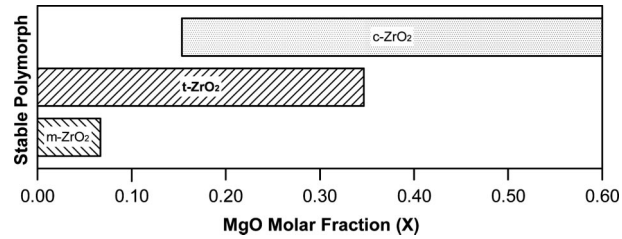

Figure 3. Representation of the relatively stability of ZrO_2 polymorphs as a function of the MgO molar fraction for samples prepared by the polymeric precursor method and calcinated at 500 °C during 15 h. The MgO cubic stability range is not shown, but traces can already be observed for 0.50 and 0.60 molar fractions.

Table 1. XPS Quantification for the Samples Containing Different Amounts of MgO[a]

x $(ZrO_2)_{1-x}$ $(MgO)_x$	$(nMg/nZr)_{bulk}$	nMg_{1s}/nZr_{3d}	nMg_{2s}/nZr_{3d}	nMg_{1s}/nMg_{2s}
0.05	0.053	0.08	0.04	2.0
0.08	0.087	0.14	0.07	2.0
0.20	0.25	0.35	0.22	1.6
0.30	0.43	0.67	0.47	1.4
0.40	0.67	0.80	0.55	1.5
0.50	1.00	1.02	0.81	1.3
0.60	1.50	4.13	3.28	1.3
1.00				1.1

[a] nMg_{1s}/nZr_{3d} is particularly representative of Mg ion dispersion in the uppermost surface layers and nMg_{2s} /nZr_{3d} represents the inner dispersion (bulk ions).

Because surface excess is related to a surface energy decreasing, Mg should be changing the common relative thermodynamic stability of the ZrO_2 polymorphs,[4] as recently published for Al_2O_3 polymorphs,[8] in addition to diffusion mechanisms. The influence of Mg in the surface energy can be studied considering the crystallite sizes evolution as a function of Mg concentration in Figure 4. Those data reflect the broadening of the diffraction peaks with increasing Mg content observed in Figure 1. To discriminate between size and strain effects on the global X-ray broadening, Halder−Wagner plots were used (Figure 5). One observes that for x varying from zero to 0.20, the interception is close to zero, indicating that the mean lattice strain effect of these nanopowders can be neglected up to this concentration point, and in a first approximation, only size effects are responsible for the broadenings of X-ray diffraction lines.

(27) Sekulic, A.; Furic, K.; Stubicar, M. *J. Mol. Struct.* **1997**, *410*, 275.
(28) Calderon-Moreno, J. M.; Yoshimura, M. *Solid State Ionics* **2002**, *154*, 125.
(29) Bouvier, P.; Djurado, E.; Ritter, C.; Dianoux, A. J.; Lucazeau, G. *Int. J. Inorg. Mater.* **2001**, *3*, 647.
(30) Li, C.; Li, M. J. *J. Raman Spectrosc.* **2002**, *33*, 301.
(31) Li, M. J.; Feng, Z. C.; Ying, P. L.; Xin, Q.; Li, C. *Phys. Chem. Chem. Phys.* **2003**, *5*, 5326.
(32) Shukla, S.; Seal, S.; Vij, R.; Bandyopadhyay, S.; Rahman, Z. *Nano Lett.* **2002**, *2*, 989.

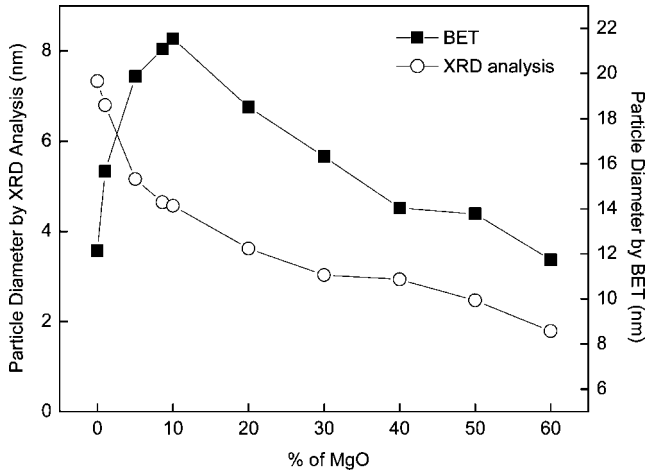

Figure 4. MgO-doped ZrO_2 nanoparticles sizes determined from BET specific surface area measurements and crystallite sizes deduced from DRX data using the Halder−Wagner method. The values differ because the BET method does not account for the grain boundary area.

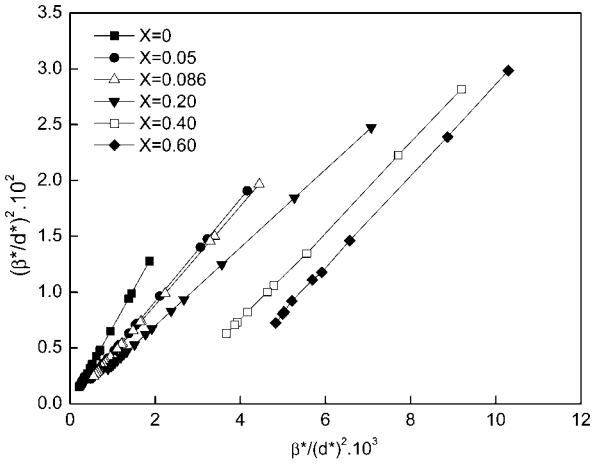

Figure 5. Halder−Wagner plots of of $(ZrO_2)_{1-x}$ $(MgO)_x$ nanopowders with different x values. The intercept of the plot gives the mean lattice strain.

Therefore, one may conclude from Figure 4 that the crystallite size of the tetragonal polymorph decreases with increasing Mg content up to 8.6 mol% ($x = 0.08$). If one considers that the amount of monoclinic polymorph is negligible with relation to tetragonal one up to $x = 0.08$, the particle size evolution of tetragonal phase can be described throughout the Ostwald ripening approach[14]

$$a^n - a_0^n = kt, \quad \text{where } k = \frac{3D\gamma c_0 M}{4\rho RT} \tag{3}$$

where a is the particle radius, t is the time of thermal treatment, D is diffusion coefficient, γ is the surface energy, M is the molar mass, R is the gas constant, T is the temperature, ρ is the density, c_o is equilibrium solubility, and n is a kinetics factor. This equation can be reasonably applied since all compositions were synthesized and heat-treated until equilibrium particle sizes were achieved (15 h).[33]

Ionic dopants may influence both the diffusion coefficient (D) and surface energy (γ) in the k factor.[34] For ZrO_2-doped powders prepared by the liquid precursor method, MgO should increase with D because of oxygen vacancies according to the equation

$$\text{MgO} \xrightarrow{\text{ZrO}_2} \text{Mg}_{\text{Zr}}^{\shortparallel} + V_{\text{O}}^{\bullet\bullet} + \text{O}_{\text{O}}^{\times} \tag{4}$$

Table 2. S_{BET} and He picnometry density of Zirconia-based Powders Containing MgO

x $(ZrO_2)_{1-x}$ $(MgO)_x$	S_{BET} (m^2/g)	density (g/cm^3)
0.000	90.4 ± 0.2	5.47
0.010	71.9 ± 0.3	5.33
0.050	57.6 ± 0.5	5.24
0.086	53.5 ± 0.5	5.32
0.100	54.5 ± 0.3	5.11
0.200	66.1 ± 0.2	4.90
0.300	79.0 ± 0.3	4.66
0.400	101.4 ± 0.4	4.22
0.500	119.6 ± 0.1	3.64
0.600	128.9 ± 0.1	3.97

One may consider that MgO decreases the surface energy, decreasing the final equilibrium particle size. This makes sense if one considers MgO is segregated as surface excess, according to eq 1, as detected by XPS and still supported by the fact that shifting on the diffraction peaks could not be detected up to 8.6 mol %, suggesting little or no solid solution.[33] A semiquantitative analysis may be carried out using eq 3 to calculate the relative surface energies. To ensure reasonable results, calculations were restricted to samples containing 5, 8.6, and 10 mol %, where only tetragonal polymorph could be observed. In the calculations, the diffusion coefficients for all samples were considered to be mostly dependent on oxygen vacancies, which concentrations depend on the molar ratio presented in eq 4. Crystallite sizes obtained from XRD data and densities of the samples measured by helium picnometry to be used in the calculations are shown in Table 2.

The calculations led to the expected surface energy decreasing: the surface energy of ZrO_2 containing 8.6 mol % MgO ($\gamma_{0.086}$) was calculated to be 0.4 $\gamma_{0.05}$. On the other hand, $\gamma_{0.10}$ (ZrO_2 containing 10 mol % MgO) was very close to $\gamma_{0.086}$, suggesting that the surface should be close to a saturation coverage. The effect of MgO in decreasing the surface energy as surface excess has been proposed previously,[7] and a maximum surface coverage has been stated as 8.1 mol %. This is consistent with the presented relative surface energy results and suggests that higher concentrations of MgO in t-ZrO_2 would be forced to go into solid solution or segregate as MgO second phase. As observed in Raman spectra shown in Figure 2, for MgO contents higher than 0.086, c-ZrO_2 becomes stable. Therefore, one may conclude that part of the Mg ions is going in solid solution and this would decrease the relatively high bulk energy, increasing the relative stability of the cubic polymorph with relation to t-ZrO_2. In fact, the solid solution hypothesis is reinforced when observing that Figure 1 shows significant shifting on the reflection peaks of cubic phase with increasing MgO content. Despite the solid solution, XPS data still detected Mg surface excess even when the cubic polymorph is stable. This is also reflected on the crystallite size measurements that, in a similar way to t-ZrO_2, show a decreasing size with

(33) Castro, R. H. R.; Hidalgo, P.; Muccillo, R.; Gouvea, D. *Appl. Surf. Sci.* **2003**, *214*, 172.
(34) Pereira, G. J.; Castro, R. H. R.; Hidalgo, P.; Gouvea, D. *Appl. Surf. Sci.* **2002**, *195*, 277.

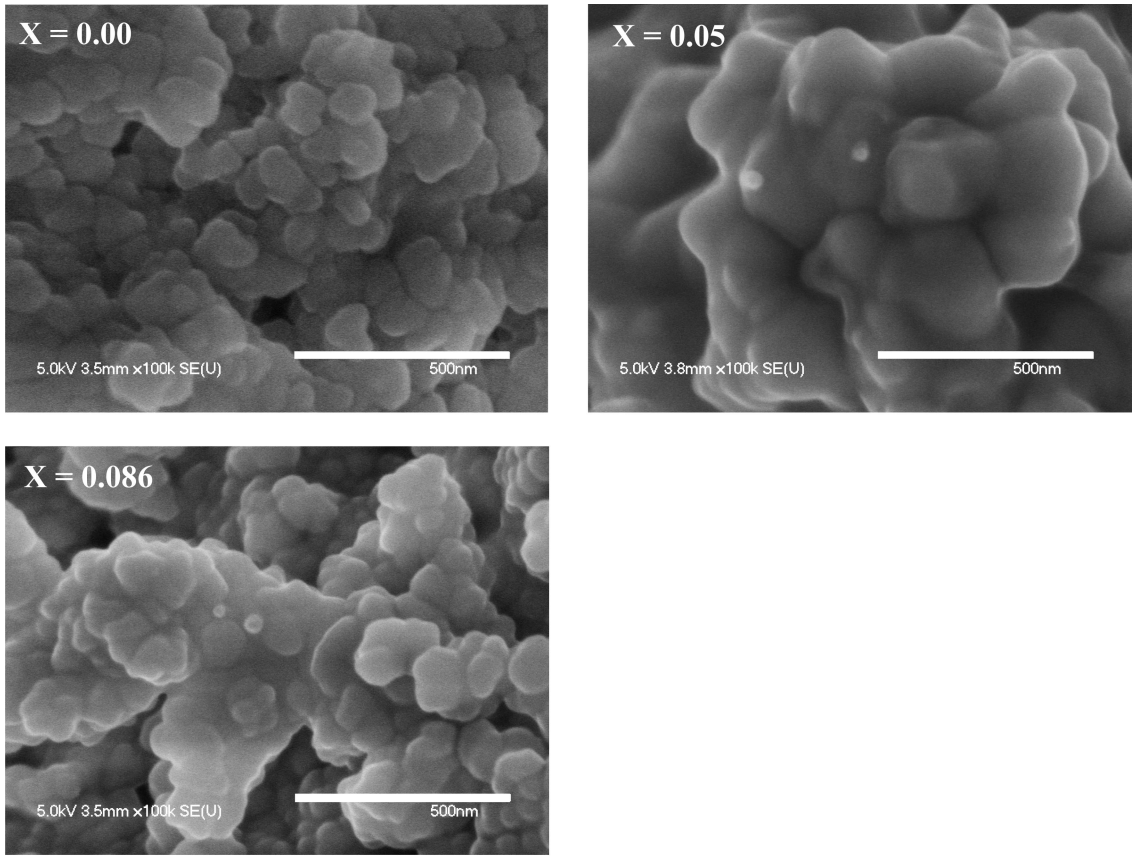

Figure 6. SEM micrographs of $(ZrO_2)_{1-x}$ $(MgO)_x$ nanopowders with $x = 0.000$, 0.050, and 0.086. One may observe sintering phenomena even at a low temperature of heat treatment (500 °C).

increasing Mg content, suggesting that despite the solid solution, Mg surface excess is still controlling the grain growth.

Table 2 also shows the specific surface area and density of ZrO_2 nanoparticles as a function of MgO content. Interestingly, one observes a surface area decreasing with increasing MgO content up to 10 mol %. This is a contradictory data when observing the crystallite data presented in Figure 4. In fact, the crystallite sizes calculated from BET do not match those from XRD line-broadening analysis. One may suggest that this anomalous behavior is related to a sintering phenomenon despite the low temperature of the thermal treatment (500 °C). Figure 6 shows SEM micrographs of the analyzed powders. Unfortunately, we could not observe the particles themselves using this technique, but only large agglomerates. Nevertheless, the SEM micrographs suggest neck formation between those agglomerates, indicating the supposed sintering phenomenon that could explain the previous presented results (HRTEM micrographs should be carried out in a future work to prove this hypothesis). This could be a consequence of the effect of Mg in grain boundary energy, resulting in higher thermodynamical potential for densification, as reported previously.[35–37]

For samples with $x > 0.1$, an increasing surface area with increasing MgO content can be observed. Because in these cases c-ZrO_2 with only traces of t-ZrO_2 are observed (Figure 2), according to the Ostwald ripening model (eq 3), whereas the diffusion coefficient increases because of the Mg solid solution, a surface energy decrease should also be accomplished to provide the surface area increase, because porosity or cavernous surface cannot be observed on ZrO_2 particles (Figure 6).

In fact, one must note that the presented discussion is valid mostly if the particle size distribution is very homogeneous. Unfortunately, the presented SEM could not show individual particles to prove this condition. However, the used synthesis method (Pechini) is well-known to provide highly homogeneous and monodispersed nanoparticles.[38] TEM image of the pure ZrO_2 nanopowder is shown in Figure 7. Despite being limited to a small region of the sample, the figure suggests that the particles are isotropic and near monodispersed, reinforcing the reliability of the presented discussion. Laser scattering to check the particle size distribution could not provide reasonable results because the particles were very agglomerated, as shown in SEM and TEM images.

Conclusion

ZrO_2 nanopowders containing MgO as additive were synthesized by a liquid precursor method and showed a

(35) Castro, R. H. R.; Pereira, G. J.; Gouvea, D. *Appl. Surf. Sci.* **2007**, *253*, 4581.
(36) Gouvea, D.; Castro, R. H. R. *Appl. Surf. Sci.* **2003**, *217*, 194.
(37) Shi, J. L. *J. Mater. Res.* **1999**, *14*, 1389.
(38) Cao, G., *Nanostructures and Nanomaterials: Synthesis, Properties, and Applications*m 1st ed.; Imperial College Press: Danvers, MA, 2004; p 433.

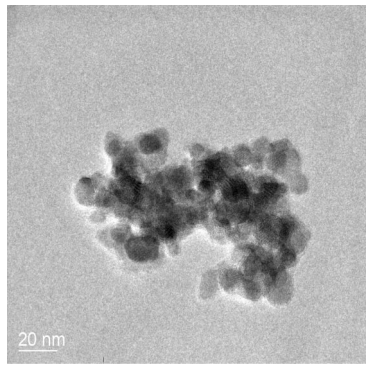

Figure 7. TEM image of pure ZrO_2 nanopowder synthesized by the Pechini method and heat treatment at 500 °C. The image suggests that the particles are very isotropic and monodispersed.

strong microstructural dependence on the MgO content. This dependence could be related to Mg surface excess, with consequent surface energy decrease, that changes the relative ZrO_2 polymorphs thermodynamic stability, which is a function of the ration between surface and bulk enthalpies.

Up to 10 mol % MgO, the surface excess promoted a stabilization of the tetragonal polymorph reducing the surface energy of this polymorph until saturation coverage was achieved. Mg solid solution was observed only after this coverage and was interestingly accomplished with the stabilization of the cubic polymorph, revealing a bulk energy decreasing, since the surface excess remained the same. Crystalline MgO, as periclase or other phase, was not observed on the X-ray diffraction patterns up to 60 mol %.

Acknowledgment. This work was supported by FAPESP (Processes 1999/10798-0, 2005/55335-0 and 2005/53241-9) and CAPES. The authors thank Dr. Reginaldo Muccillo, from Instituto de Pesquisas Energéticas e Nucleares, São Paulo, Brazil, for the X-ray patterns presented in this paper.

CM703599R